

Research Paper

Cite this article: Roja V, D. SK (2023). Radio wave propagation analysis with dominant path model using MIMO antenna element for vehicular base station application.

International Journal of Microwave and Wireless Technologies **15**, 1789–1800. <https://doi.org/10.1017/S1759078723000557>

Received: 16 September 2022

Revised: 11 April 2023

Accepted: 14 April 2023

Keywords:

base transceiver station; dual-polarized antenna; high isolation; machine to machine; wireless communication

Corresponding author: Vadlamudi Roja;

Email: vadlamudi93@gmail.com

Radio wave propagation analysis with dominant path model using MIMO antenna element for vehicular base station application

Vadlamudi Roja  and Sriram Kumar D.

Department of ECE, National Institute of Technology, Tiruchirappalli, India

Abstract

A low-profile slant $\pm 45^\circ$ polarized antenna for a 4G/5G base station with a dominant path wave propagation model (DPM) is reported in this paper. For dual-polarization and wide impedance bandwidth, the two dipole radiators are crisscrossed and a square metallic ring is integrated with the dipole arms and screwed with the four shorting vias. The antenna operates in Band 40/41/42/43 with strong isolation and low ECC (Envelope Correlation Coefficient). Fabricated antenna results show that the predicted wideband antenna has 13.38% bandwidth in 4G, which is Band 40/41, and 29.33% bandwidth in 5G sub-6 GHz Band 42/43. The antenna has a consistent radiation pattern, a 40 dB XPD (Cross Pol Discrimination), and a beam width of $69.5^\circ \pm 1.5^\circ$ in the entire frequency band. Three base station sites were explored to deploy the radiation pattern of a dual-polarized antenna in the 3D EM (Electromagnetic Analysis) tool. To evaluate signal quality, strength, radio network planning, and wave propagation analysis by analyzing antenna performance in real-time scenarios with 64 and 256 QAM (Quadrature Amplitude Modulation) techniques. For the proposed four-stream MIMO (Multiple-Input-Multiple-Output) antenna arrangement at deployed cell sites for 4G/5G base station applications, the maximum downlink and uplink data rates are 3.826/2.8 Mbps and 1044/800 Mbps respectively.

Introduction

With the growth of fifth-generation (5G) technology, the number of users (user equipment [UE], machine-to-machine [M2M], IoT (Internet of Things), vehicle-to-vehicle [V2V], etc.) using 5G services is increasing exponentially. High throughput is required to provide the 5G service to the users in upcoming dense urban and rural areas; hence, the motivation to install the MIMO Base Transceiver Station (BTS) antenna is a tangible task. As per the third-Generation Partnership Project (3GPP), International Telecommunications Union (ITU) fixed and named the mid-band as frequency range-1 band or sub-6 GHz band ranging from 410 to 7125 MHz for 5G network deployments [1]. Operators, however, demand low-profile and lightweight antennas for ease of installation in 4G and 5G base station towers [2, 3]. A pictorial representation of the vehicle-to-infrastructure, vehicle-to-everything, M2M, and V2V wireless communication is shown in Fig. 1(a). Each vehicle can talk to other vehicles on the road, base stations, the driver, and passengers. A cellular base station antenna with wideband high-gain properties is desirable to meet different communication requirements with multiple communication network deployments. When addressing two or more wireless communication applications, increasing the impedance bandwidth and reducing the interference through various MIMO antenna elements become difficult.

The network infrastructures of all generations from 2G to 4G, including the core network, base band unit (BBU), and radio remote head (RRH), are on the ground surface, with only antennas installed on the towers. The RRH, BBU, and the heat sink are called the radio unit (RU). The RU and the antennas are in one enclosure, called an active antenna system (AAS). As per 3GPP-ITU recommendations, the 5G network deployment demands a compact AAS on the cell phone tower, as shown in Fig. 1(b). As a result, the design challenge for 5G technology is to create attractive antenna features with a low profile and lightweight that is suited for both 4G and 5G deployment. The compact antenna system replaces the existing 3G/4 G antennas and satisfies all generations [4]. Bandwidth, gain, and isolation enhancement are done using artificial magnetic conductor (AMC) cavity, parasitic elements, and vertical stubs in the design [5–7]. Frequency selective surface is introduced to eliminate the influence of the Low Band (LB) antenna on the Mid Band/High Band (MB/HB) antenna array and to get the wideband-Band-pass filter response [8]. The dual-band performance is achieved by integrating a small oval-shaped loop within the large oval-shaped loop without increasing the size of the radiating patch [9]. Many attempts have been made to design dual- or multi-band

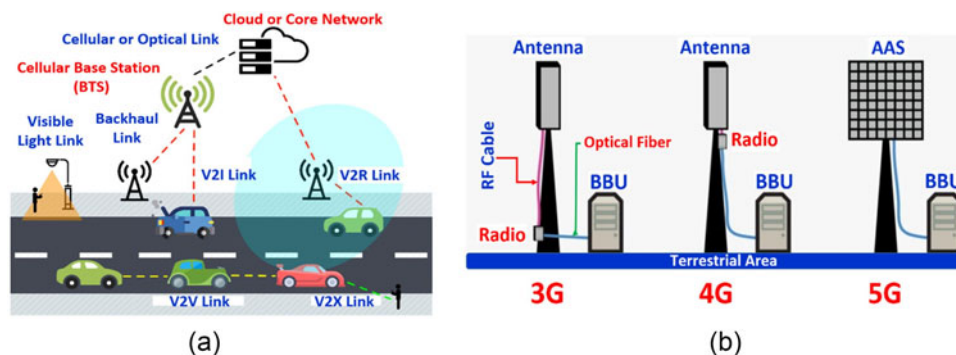


Figure 1. Pictorial representation: (a) wireless communication networks and (b) network architecture evolution.

antennas for miniaturized base station applications. In [10], the adaption of the vector synthesis technique provides better isolation and low cross-polarization. An arrangement of probe-fed annular ring elements and pairs of cross microstrip dipoles nested together makes the design more complex. A differential feeding mechanism provides antenna miniaturization, thereby, a low profile [11].

A cascaded coupled-resonator decoupling network can effectively mitigate the coexistence between two co-located systems by providing at least 20 dB of isolation improvement and enhanced matching performance [12]. The high-frequency radiators are positioned over the low-frequency patch in this scheme [13], which makes the design more intricate. Stack-up configurations indirectly increase the overall antenna height, which is not practically desired for deployment. Even though [14] AMC is used to address the issues of size and wideband, the infinite ground plane is limited to achieving the 0° reflection phase with low backfiring. In [15], both dual-band antennas are printed on opposite sides of the substrate. This scheme provides good radiation characteristics but usually suffers from cross-polar discriminations (XPD) of more than 20 dB at 0° and more than 10 dB at $\pm 60^\circ$.

This paper presents a novel approach that allows low-profile, dual-polarized, high isolation base station antenna to address the challenges in outdated methods reported in the literature [16]. The two dipole radiators are placed in crisscross arrangement to obtain the wide impedance bandwidth. A square metallic ring with a 3 mm air gap is placed below the dipole arms connected with four shorting vias to operate the antenna in Band 40/41/42/43. The overall antenna height, including the radome, is only 0.25λ (λ at an operating wavelength of 3.5 GHz), smaller than the state-of-the-art designs [17]. Ansys HFSS 3D EM solver is used for the antenna design and simulation [18]. A dual slant $\pm 45^\circ$ polarized dual-generation antenna is fabricated and tested.

This paper is divided into six sections: “Design of a dual-generation MIMO antenna element,” which deals with design flow, starting with radiator selection in terms of critical parameters, antenna design, and feeding techniques; “Results and discussion,” “Radio network planning for 4G and 5G MIMO antenna,” “Wave propagation analysis using 4G and 5G MIMO antenna,” and “Conclusion.”

Design of a dual-generation MIMO antenna element

A flared bow tie structure of length $\lambda_0/2$ (42.5 mm) at a center frequency of 3.5 GHz is modeled. A detailed view of the wideband radiator is shown in Fig. 2. The proposed dual-polarized antenna is powered by radiofrequency (RF) cables; the inner conductor of

the cable is connected to one arm of the leaf-shaped dipole and the outer conductor is connected to another arm of the antenna. Finally, the outer layer of the RF coaxial cable along with one arm of the dipole antenna is connected to the back reflector plane. Another metal post with an RF cable connecting the other dipole arm to the ground is located in the symmetrical plane. A balun is created by the exterior part of the RF cable and the shorting metal post, which optimizes the antenna’s feed. It is clear that the patch’s edges are where the current prefers to flow the most. The current could be adjusted symmetrical with 0° directions by optimizing the lengths of the metallic post, square ring, and dipole arms. This improved the 0° linearly polarized wave and decreased the antenna’s cross-polarization. The novelty of the design lies in the fact that for acquiring the dual-polarization, the two flared petal-shaped dipole radiators are placed in a crisscross manner with wide impedance bandwidth, high isolation, and low cross-polarization. A square metallic ring with a 3 mm air gap is placed below the dipole arms and are connected with four shorting vias, as shown in Fig. 2(a) and (b). The square ring that connects the outer edges of the dipoles’ arms that makes the antenna short is another important feature of this antenna. The adjacent edges of the dipole arms form a shorted slot transmission line as the dipoles’ ends are connected. An open circuit is presented at the feeding point of the dipole by appropriately adjusting the parameters of this shorted slot transmission line. As a result, the isolation between the two polarizations is improved by decreasing the current at the feeding point. The antenna height is reduced in part due to the center’s suppression of the current.

The side length is 21.2 mm, which makes an acute angle of $a = 60^\circ$. The other working mechanism of the antenna and how the fields on the metallic ring and dipole arms contribute to the wider bandwidth at 2.5 and 3.5 GHz are illustrated in Fig. 2(c). Fig. 2(c) shows the three current traveling paths at 2.5 GHz for a -45° polarized radiator. One direction is along the dipole arms, and the remaining two paths are from the square ring to the dipole arms. The current traveling path indicates that the radiators seem like non-uniform folded dipoles to achieve multiple resonances. Similarly, at 3.5 GHz, fields are highly concentrated on the ring and less on the sides of the dipole arms.

The fields on the ring seem like the short dipole scenario, and the slant 45° polarization is obtained by the conciliation of four field paths on the square ring. The L_{arm} is calculated using equation (1),

$$L_{\text{arm}} = R * \left(1 + \frac{1}{\tan(0.5 * a)} \right), \quad (1)$$

where R is the half circle radius and a is the acute angle.

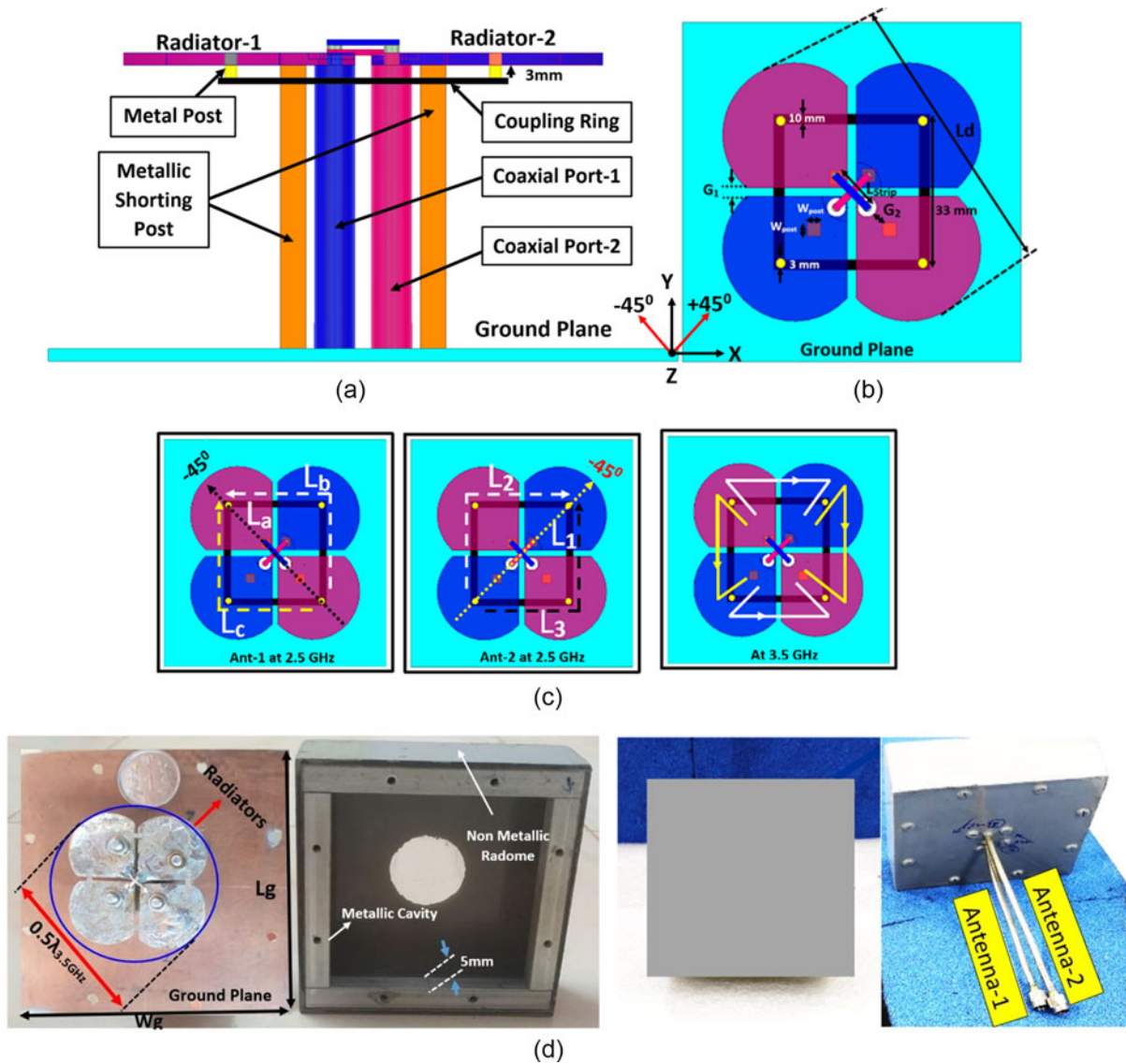


Figure 2. Configuration of the proposed low-profile dual slant $\pm 45^\circ$ polarized antennas: (a) side view, (b) top view, (c) current distribution, and (d) MIMO antenna prototype.

The square ring is placed under the dipole radiators with a 3 mm air gap and shorted with the four corners of the ring with vias because the leaf-type dipole arms are very close to each other. As the gap is smaller, the frequency range is narrower. The ring length (L_r), dipole arm length (L_{arm}), and acute angle (a) have a significant impact on the input impedance. From the above interpretation, it is noted that the primary resonance is due to the leaf-type (petal-shaped) dipole radiator, and the secondary resonance is yielded due to the cumulative impact of the square ring, which is placed 3 mm below the radiators and the mutual coupling between the flared petal-shaped dipole arms. The effect of coupling between the parallel vertical rods and the coaxial cables with squaring strip together diminish the near-field coupling between the adjacent channels. The use of additional parallel metallic vertical rods improves port-to-port isolation and reduces cross-polarization levels by locating the return current path to the ground plane. These petal-shaped bow tie radiators give a bidirectional pattern on the broadside. To get a unidirectional pattern based on image theory, a perfect electric conductor (PEC) acts as a reflector larger than the size of the radiator placed at $\lambda_0/4$ under the radiator parallel to it. A PEC

is a metallic surface and can be realized by a copper plate. This arrangement will improve the gain by two folds. The antenna is fed with an SubMiniature version A (SMA) connector to create a simple planar radiator for low-profile geometries. Table 1 compares the proposed BTS antenna with the antennas available in the literature.

Table 2 shows the comparison of the characteristics between the anticipated antenna and the research results published in recent years [5,6] and [13,16] in terms of electrical size, impedance bandwidth, isolation, gain, and feed configuration. The features of the proposed antenna are low profile, larger bandwidth, high isolation, high gain, low XPD, and stable radiation pattern.

Results and discussion

In the simulations and measurements, different orientations are considered in azimuth, elevation, and slant directions to understand the capability of simultaneously producing $+45^\circ$ and -45° multi-beam patterns.

Table 1. Optimized antenna dimensions

Parameters	Description	Values (mm)
L_g	Length of the ground plane	65
W_g	Width of the ground plane	65
L_d	Dipole length ($0.5 \cdot \lambda_{3.5\text{GHz}}$)	42.5
L_{strip}	Strip length	5
L_{arm}	Length of the dipole arm	21.2
G_1	Spacing between dipole arms	1.32
G_2	The gap between shorting post and coaxial cable	1.77
R	Semicircle radius	9.25
W_{post}	Shorting post width	3
H	The gap between the radiators and ground plane	21.53

Dual-generation dual-polarized MIMO antenna element performance

The simulated and measured S -parameters of the dual-polarized antenna are shown in Fig. 4. The developed antenna element covers the frequency band from 2 to 5 GHz ($S_{11} < -15$ dB, 42.85%). The slant $\pm 45^\circ$ polarized signals communicate well with the UE. An Agilent N9927A vector network analyzer is employed to measure the performance of the antenna. Fig. 4 presents the simulated and measured return loss showing the measured -10 dB return loss impedance bandwidth and isolation of >40 dB ranges from 2 to 5 GHz (42.85%). Discrepancies between the measured and simulated results are probably due to the additional insertion loss induced by the inclusion of the SMA connector. Besides, the simulations assign the ground plane, patch radiator, coaxial connector, and shorting pins as PEC boundaries. In contrast, they are made from lossy metals in the prototype, and the inductive effect of soldering may also contribute to the discrepancies.

The far-field radiation pattern of the prototype antenna is measured in the anechoic chamber. The measurement setup is shown in Fig. 3. The transmitter (Tx) is a standard gain horn and the receiver (Rx) is the antenna under test, mounted at 1.5 m height in the far-field separation of 3.65 m. Fig. 5(a) and (b) represent the normalized measured radiation patterns in the xz - and yz -planes at 2.5 and 3.5 GHz, respectively.

The measured results of a MIMO antenna element provide a directional stable radiation pattern and a cross-polarization level of -40 dB, front to back ratio of 23 dB, and a maximum gain of 11.3 dBi and beam width of $69.5^\circ \pm 1.5^\circ$. The slight variation in the measured radiation pattern is due to the alignment of the Rx antenna to the Tx antenna. However, the proposed antenna provides a broader beam width, which results in the wider coverage, and larger range is made possible due to high-gain properties of the antenna for telecommunication network demands.

Envelope correlation coefficient and directive gain

Because of the external environment, signal fading occurs in realistic mobile scenarios. The envelope correlation coefficient (ECC) is crucial when assessing the performance of a MIMO antenna element in typical multipath scenarios. The ECC of a MIMO antenna

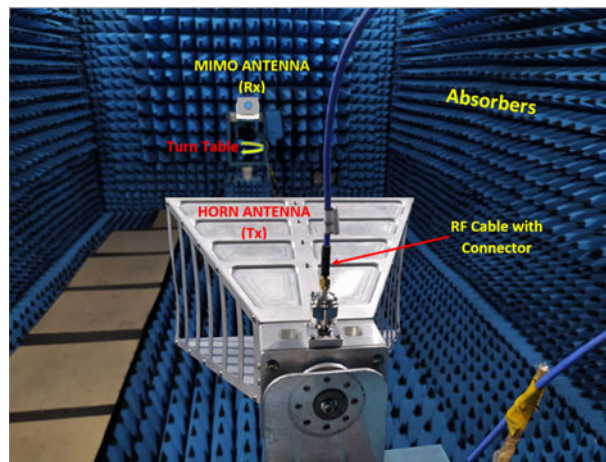


Figure 3. Fabricated dual-polarized MIMO antenna element in an anechoic chamber.

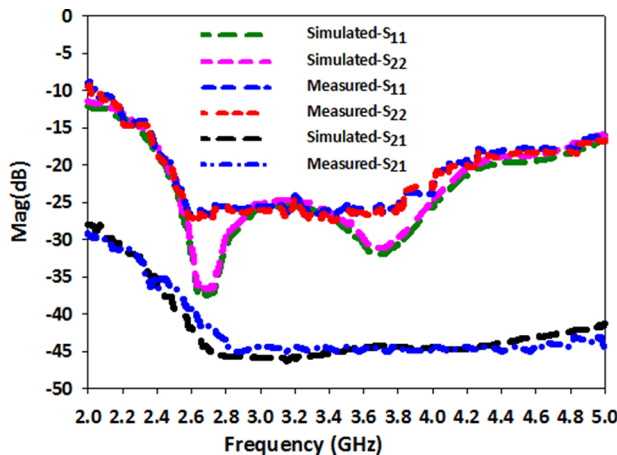


Figure 4. Simulated and measured S -parameter comparison of the proposed antenna.

element with two dual-polarized elements is assessed in this section. For a decent radiator with excitation at different antenna ports, the acceptable value of ECC should be less than 0.5. ECC (ρ_e) is calculated using measured far-field radiation patterns at the resonant frequency reported in [19] using equation (2). The ECC (ρ_e) is depicted in Figure 6(a).

$$ECC(\rho_e) = \frac{\iint_{4\pi} E_i(\theta, \phi) \cdot E_j^*(\theta, \phi) d\Omega}{\sqrt{\iint_{4\pi} E_i(\theta, \phi) \cdot E_i^*(\theta, \phi) d\Omega \iint_{4\pi} E_j(\theta, \phi) \cdot E_j^*(\theta, \phi) d\Omega}} \tag{2}$$

where $E_i(\theta, \phi)(\Omega)$ and $E_j(\theta, \phi)(\Omega)$ are complex electric fields radiated by the antenna fed with two different ports along θ and ϕ direction and Ω is the solid angle.

The maximum ECC value obtained in Band 40 is 0.05. On the other hand, the maximum ECC values range from 0.01 to 0.0001 in Band 41/42/43. The above results prove that the radiation patterns of both antennas are uncorrelated.

Furthermore, diversity gain (DG) [20] is another important parameter to evaluate the MIMO antenna element performance,

Table 2. Comparison of proposed BTS antenna with literature

Reference	Polarization/feed	Operating frequency (GHz)	Isolation/XPD (dB)	Overall antenna size (mm ³)	Maximum measured gain (dBi)
[5]	Dual/Printed	0.69–0.9/1.71–2.69	20–32/20–25	$3.33\lambda_0 \times 3.33\lambda_0 \times 0.94\lambda_0$	8.0
[6]	Dual/Coaxial	2.5–2.690/3.3–3.6	38/25	$0.43\lambda_0 \times 0.43\lambda_0 \times 0.26\lambda_0$	8.5
[13]	Dual/Printed	2.35–4.25	28	$1.13\lambda_0 \times 1.13\lambda_0 \times 0.26\lambda_0$	9.65
[16]	Dual/Printed	2.38–2.54/3.11–4.15	28/23	$0.8\lambda_0 \times 0.8\lambda_0 \times 0.27\lambda_0$	3.9/7.2
Proposed antenna	Dual slant ($\pm 45^\circ$)/Coaxial	2.0–5.0 band 40/41/42/43	40/40	$0.55\lambda_0 \times 0.55\lambda_0 \times 0.25\lambda_0$	11.3

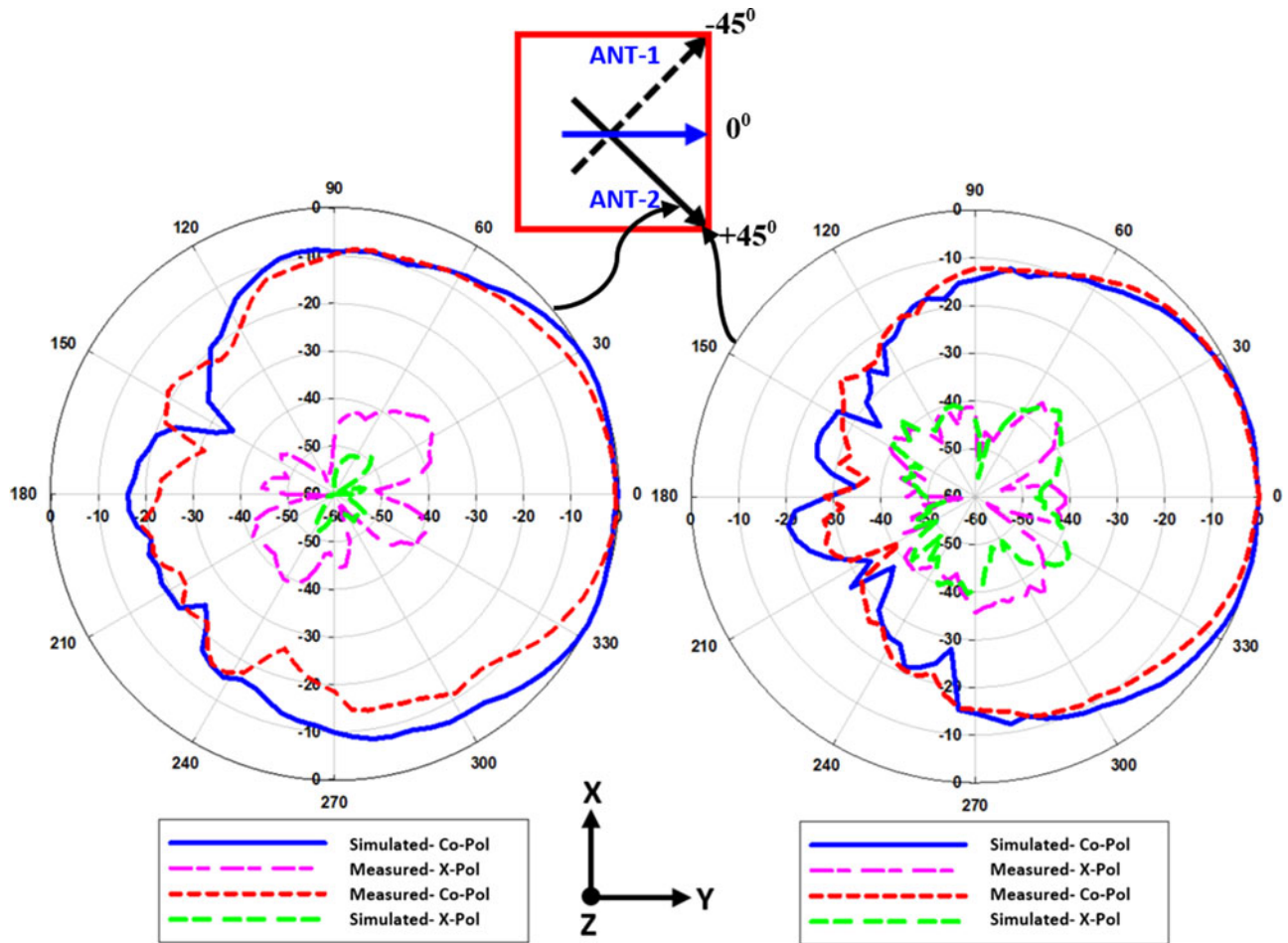


Figure 5. Radiation patterns of dual-generation dual-polarized MIMO antenna element ($+45^\circ$) are excited: (i) 2.5 GHz and (ii) 3.5 GHz at the broadside direction.

which is calculated using equation (3). Fig. 6(b) shows a proposed MIMO antenna’s simulated and measured DG. It is noted that the DG is close to the ideal case’s maximum value in the operating bands.

$$DG = 10 * \sqrt{1 - |\rho_e|^2}. \tag{3}$$

Radio network planning with 4G and 5G MIMO antenna

The dual-polarized MIMO antenna element is designed using the FEKO-WinProp software for the 4G and 5G BTS applications in the real world by setting various air interface wireless standards. The DP antenna design uses the FEKO-WinProp 3D EM software

package, which provides ray-tracing models with 3D visualization of actual deployment in campus environments. The WinProp software, which also supports numerous wireless technologies with 3GPP specifications, considers the effects of many characteristics such as reflection, refraction, scattering, path loss, and line of sight.

The ray-tracing models in WinProp [21] facilitate the analysis of 3D building information describing the provided surroundings while considering all the predominant wave propagation features (reflection, diffraction, and scattering). The propagation models incorporate all 3D object data, making them three-dimensional. The dominant path model (DPM) combines high accuracy with rapid computing and provides accurate predictions for radio coverage. The systematic deployment procedure for the proposed

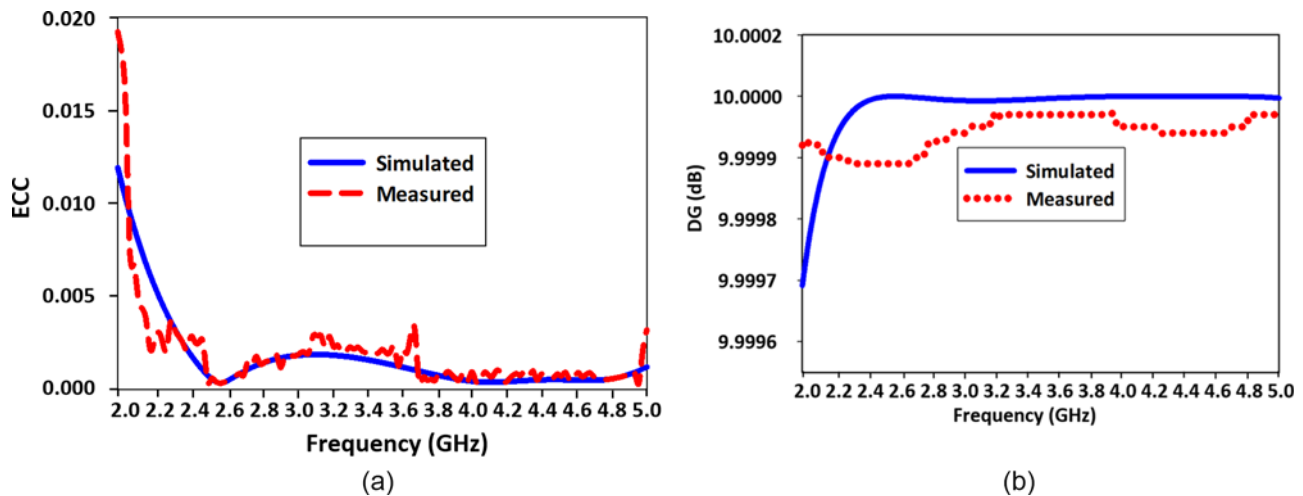


Figure 6. (a) ECC and (b) DG of the proposed antenna.

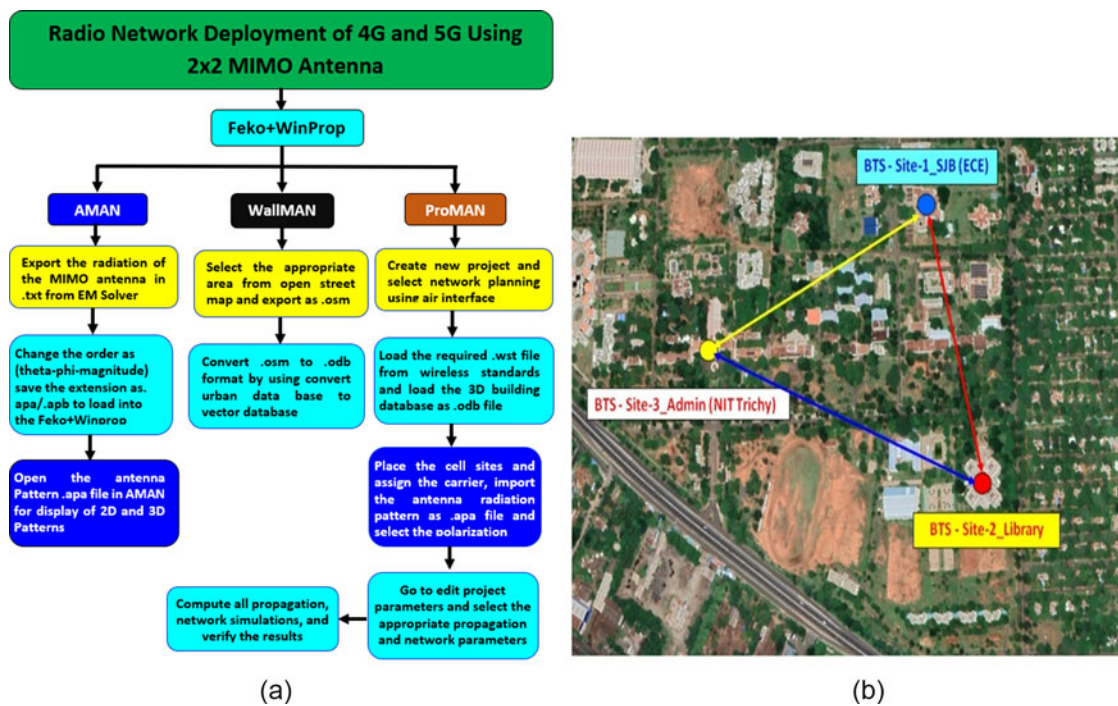


Figure 7. (a) Flowchart for the 4G/5G MIMO antenna deployment in the WinProp environment. (b) Three locations of BTS Sites 1, 2, and 3 at the NITT campus with respective departments are marked on the map.

4G and 5G MIMO antenna is shown in Fig. 7(a). The campus of the National Institute of Technology Tiruchirappalli (NITT) is chosen for deploying the developed MIMO antenna element on graphical terrain with BTS Sites 1, 2, and 3, as depicted in Fig. 7(b). The equivalent 3D vector-building database of the selected urban environment using WallMan is shown in Fig. 8(a).

Antenna manager (AMAN) is used to export the designed radiation patterns for the MIMO antenna element from the 3D EM simulators and make them compatible with WinProp. In order to export the 3D radiation pattern data in terms of Theta and Phi from 3D EM solvers and save as .apa/.apb file format and export the same file into WinProp platform for the 3D radiation pattern of the MIMO antenna. Figure 8(b) illustrates the 3D radiation

pattern of the MIMO antenna. This simulation tool offers various three-dimensional methods by considering 3D object data when computing all rays in 3D. To deploy cell sites in specific geographic terrain, the ProMan (Project Manager) is used, and necessary network planning is carried out through various air interfaces.

Any highly populated metropolitan region can choose the MIMO antenna element deployment with various configurations; for convenience, the NIT Tiruchirappalli campus perspective is considered and examined. The simulations are performed at three different sites, identified on the map as BTS Sites 1, 2, and 3 (Silver Jubilee Building (SJB), Department of ECE, Central Library, and Administration Building, respectively), with inter-site distance of 700 m from BTS Sites 1 and 2 and 850 m from BTS Sites 2 and 3.

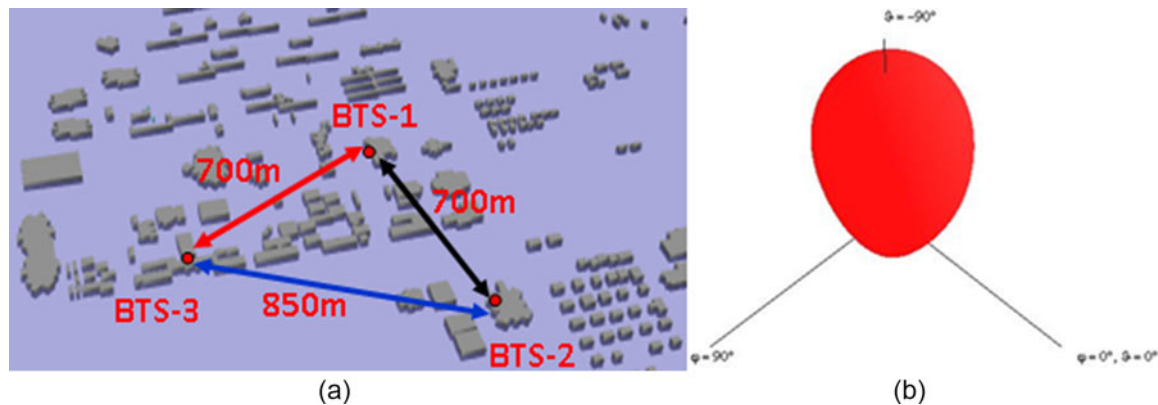


Figure 8. (a) 3D vector-building database of a selected urban environment in WallMan and (b) 3D radiation pattern in AMAN.



Figure 9. The isometric view of the buildings in the NITT campus is marked as (a) Site 1, (b) Site 2, and (c) Site 3 in the cell site area.

Figure 9(a–c) shows an isometric view of the buildings as indicated on the map. These places are selected so that the deployed MIMO antenna element can see the various environments and address the highest number of users. BTS Sites 1, 2, and 3 are deployed at an altitude of 25 m from the terrace in the designated MIMO antenna element configurations to maintain uniform coverage. Different MIMO antenna element configurations are explored by utilizing the dominant path model.

Wave propagation analysis using 4G and 5G MIMO antenna element

The effectiveness of the network's architecture determines how well wireless communication networks perform. Radio network planning is crucial to assess the wireless network performance due to the broad range of accessible air interfaces for cellular and broadcast wireless networks [21] with their diverse behavior and parameter settings. To provide high-speed data rates for 4G and 5G deployments, ultradense networks comprising base stations with minimal power in suburban areas are used. Therefore, a rapid coverage prediction model is necessary. Here, the dominant path model is used for Band 41 (2.496–2.690 GHz) 4G and Band 42 (3.4–3.6 GHz) 5G radio planning, combining high accuracy with minimal computing time. All cells with Tx antennas above, below, or on the rooftop can use the DPM, which enables a broad frequency range. Tables 4 and 5 summarize radio coverage with the DPM for various air interface wireless technologies.

WinProp tool determines the downlink (DL) and uplink (UL) data rates, throughputs, signal-to-noise plus interference ratio

(SNIR), Reference Signal Received Power (RSRP), Reference Signal Received Quality (RSRQ), Received Signal Strength Indicator (RSSI), received power, path loss, and the coverage area for each transmission mode. Both time division duplex (TDD) and frequency division duplex (FDD) technologies are used for 4G (Band 41) and 5G (Band 42), according to the tabulated statistics. In FDD, UL and DL use different frequencies, whereas in TDD, UL and DL transmit on the same frequency but at different time intervals.

Generally, TDD is preferred for better capacity, whereas FDD is used for better coverage. However, the 5G FDD standards with a dual-polarized MIMO antenna element composed of three locations are selected by analyzing the results and the coverage area over the selected region. Fig. 10(a) depicts the cell areas across the map chosen; Site 1 coverage is represented in green color, Site 2 in red color, and similarly Site 3 in blue color. Based on simulation results, each cell site's path loss is determined to be -90 dB, as shown in Fig. 10(b).

The results are more precise and realistic because the DPM adopts a fully 3D approach in path searching. This model identifies the one dominating path between each transmitter and receiver pixel. Compared to ray-tracing models, the computing time is significantly less, and the accuracy is identical to that of the knife-edge diffraction model. A DPM is preferred because ray-tracing models require a lot of time and depend upon the vector databases that subsequently affect the accuracy. The most significant propagation path between transmitter and receiver is determined by DPM, which contributes more than 90% of the total energy. As a result, computation time is reduced, and accuracy is nearly on par with ray-tracing models [22].

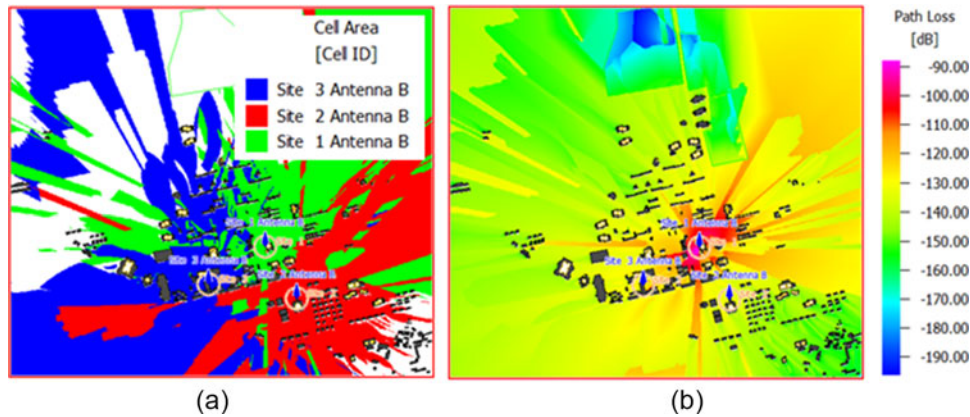


Figure 10. Simulation results of (a) cell area and (b) path loss over the selected area from the map.

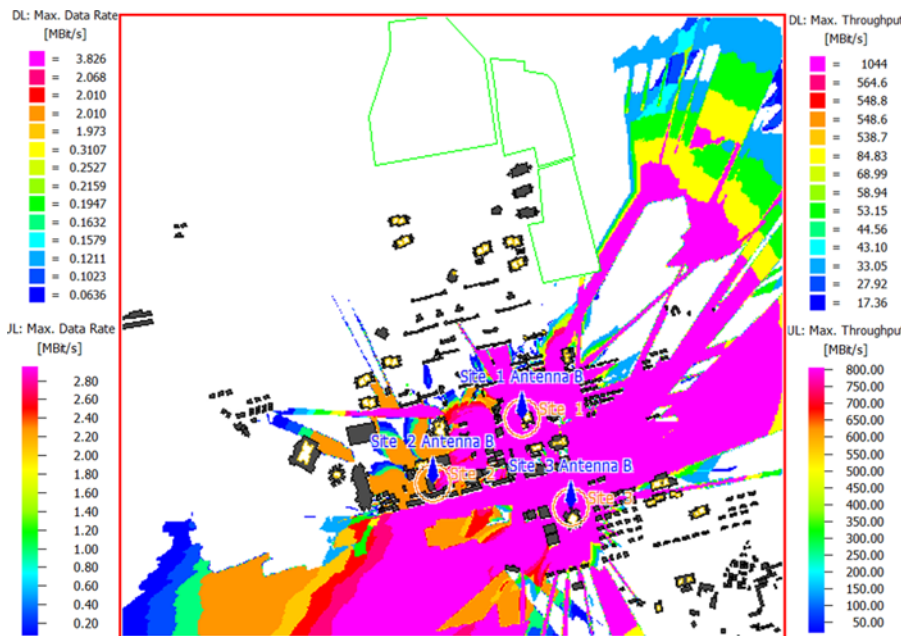


Figure 11. Downlink and uplink: max. Throughput and data rate with dominant path model for the MIMO antenna element.

The DPM model is the best method for computing coverage predictions in significant urban areas because it does not require preprocessing for vector databases. The following equation is used to determine the computation path loss (L) [23],

$$L = 20 * \log\left(\frac{4\pi}{\lambda}\right) + 10 * p * \log(l) + \sum_n^{i=0} f(\varphi, i) + \Omega + g_t, \quad (4)$$

where L is the path loss (dB), l is the distance between the Tx and Rx, p is the path loss factor, f is the loss (dB) component due to the diffraction, λ is the wavelength at the operating frequency, g_t is the transmitting (Tx) antenna gain (dB), and Ω is the wave guiding component that determines the gain values. The wave guiding factor depends on the reflection loss due to the guiding walls and their distance to the wave propagation path. The maximum input power (P_T) given to the macro cell base station MIMO antenna element is 48 dBm or 69 W at the antenna connector. The developed MIMO BTS antenna gain (G_T) is 10 dBi, the maximum connector loss (L_C) of the antenna is considered 1 dB, and cable loss is 0 dB (ideal case). The maximum effective isotropic radiated

power (EIRP) is calculated using the below equation [24] at the transmitting antenna aperture as 57 dBm:

$$EIRP = G_T + P_T - L_C. \quad (5)$$

Figure 11 shows the four-stream data rates and throughput for both the UL and the DL. According to Fig. 12(a), the maximum SNIR and received power are 50 dB and -50 dBm, and Fig. 12(b-d) show the signal quality and strength parameters RSRQ, RSRP, and RSSI for a MIMO antenna element.

The simulation results show that the signal strength is excellent across the entire map with selected base stations at Sites 1, 2, and 3, with a maximum RSRP of -75 dBm, RSRQ of -4 dB, and RSSI of -40 dBm. In conclusion, from the above extensive simulation studies, it is observed that the high isolation BTS antenna provides high data rates and throughputs for the 4G and 5G network deployment. According to the Shannon channel capacity theorem, channel capacity is defined as a theoretical maximum bit rate (number of bits/s) for the noisy channel. This channel capacity is

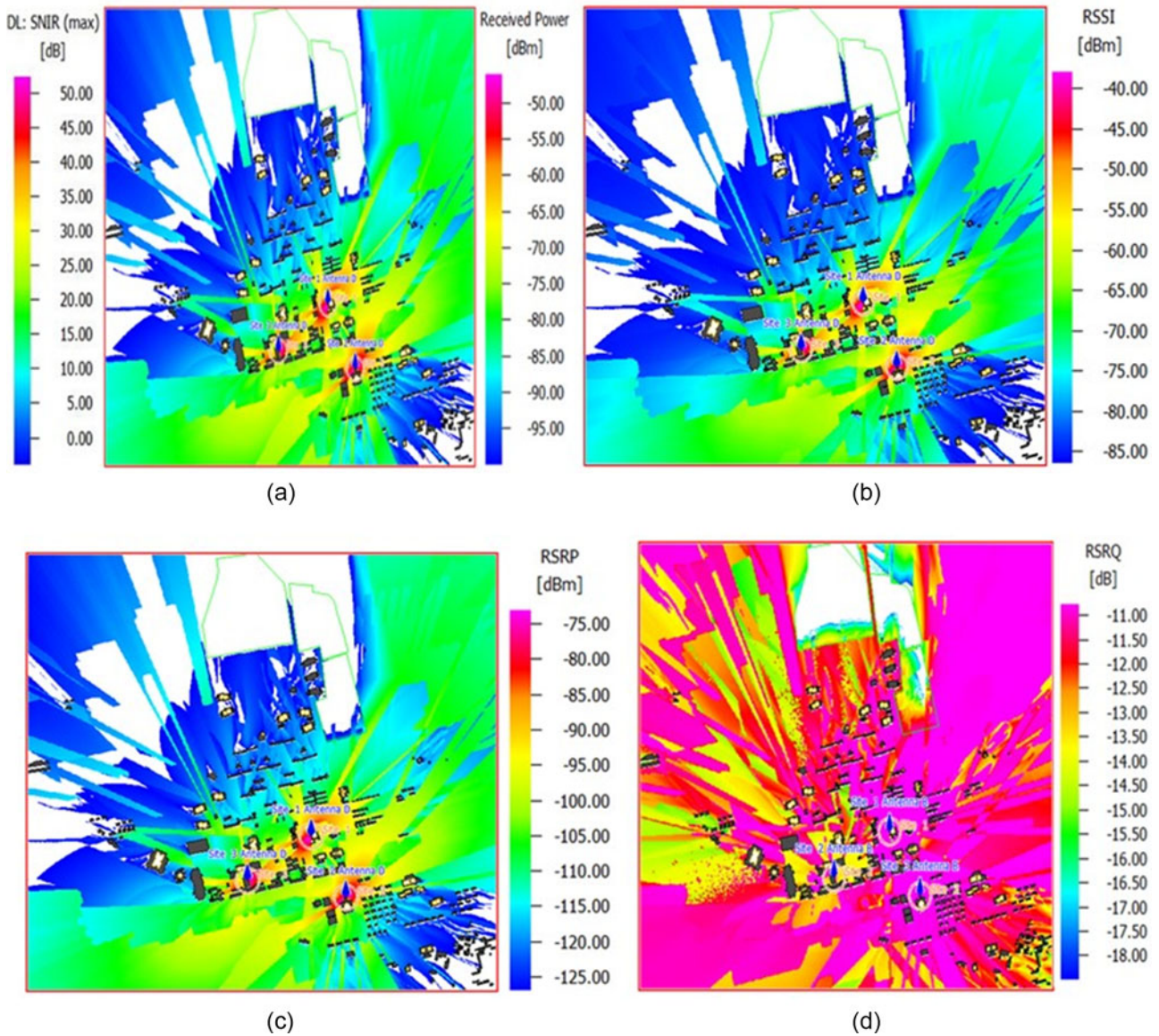


Figure 12. (a) SNIR and received power, (b) RSSI, (c) RSRP and (d) RSRQ for the map area with the dominant path model for the MIMO antenna element.

calculated using the following equation [25]:

$$\text{Channel Capacity (C)} = \text{BW} * \log_2 \left(1 + \frac{S}{N} \right) \quad (6)$$

where BW = channel bandwidth, S = signal power (watts), and N = noise power (watts).

As per the above equation, maximum channel capacity or maximum data rate can be achieved only when the channel's bandwidth or SNIR is higher. The SNIR of the MIMO system is increased if an antenna has high isolation (polarization diversity) and low XPD, as shown in Table 3. Polarization diversity uses the antennas of different polarization, i.e., slant $\pm 45^\circ$. If the low isolation dual-polarized antenna is used for the wireless communications, then the adjacent channel interference or the channel leakage ratio increases and thereby a cross-talk occurs, which disturbs the entire communication systems. So, many of the telecom operators prefer to take high isolation BTS antennas for efficient network communications to provide quality of service to the users. Also, high isolation antennas improve the spectral efficiency of

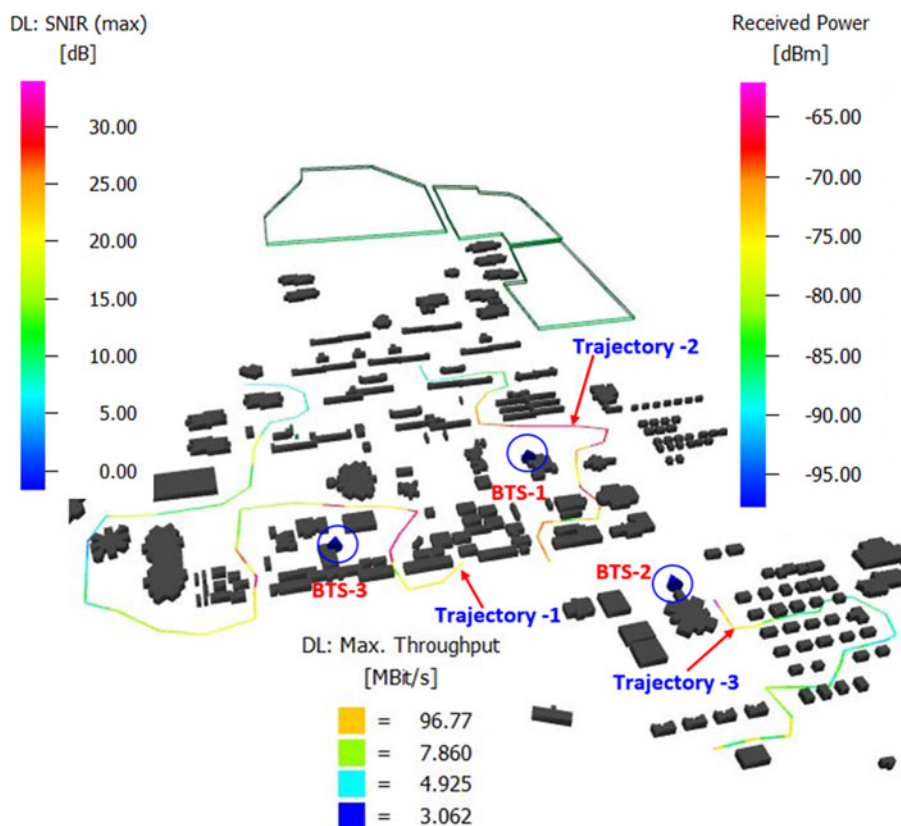
the network for better services to the end users. The MIMO antenna uses multipath propagation characteristics to receive separate uncorrelated signals. The rigorous studies show that the antenna with high isolation reduces the interference and improves the SNIR. As a result, data rate and throughput increase. In addition, it is concluded that the antenna with high isolation provides high data rates and throughput in the specified channel bandwidth (20 MHz for 4 G and 100 MHz for 5G).

In a typical propagation analysis, the orientation of the receiving antenna concerning the geometry's coordinate system is specified. But when the receiving antenna is fixed to a vehicle, it moves with the vehicle. As a result, one establishes a trajectory in a virtual drive test. As it travels along the trajectory, the receiving antenna's orientation changes by its motion.

The received power, SNIR of 30 dB, maximum throughput of 96.77 Mbps, and received power of -65 dB for this particular scenario are plotted in conjunction with propagation or network analysis for the selected geographical area as shown in Fig. 13. The

Table 3. Comparison of channel capacity parameters of the antenna with low isolation and high isolation

S. no.	Parameters	As per 3GPP expected values	5G			
			TDD		FDD	
			20 dB isolation	40 dB isolation	20 dB isolation	40 dB isolation
1	Received power (dBm)	—	-55	-50	-53	-50
2	DL: data rate (Mbps)	—	1.05	1.913	2.1	3.826
3	DL: throughput (Mbps)	—	255.3	522.2	510.5	1044
4	UL: data rate (Mbps)	—	0.59	1.473	1.43	2.75
5	UL: throughput (Mbps)	—	198.3	402.3	412.3	800
6	Max. SNIR (dB)	≥ 20	37	45	45	50
7	RSRP (dBm)	≥ -80	-75	-75	-75	-75
8	RSRQ (dB)	≥ -15	-11	-4	-11	-4
9	RSSI (dBm)	≥ -65	-50	-40	-50	-40
10	Path loss (dB)	≤ -80	-85	-90	-90	-90

**Figure 13.** The receiving antenna moves along the trajectory in the specified path.

comparison of radio network parameters with three wave propagation model and with various MIMO streams are reported in Table 3, and it is clear that the DPM model provides accurately network parameters with less simulation time. Before installation of base station towers, this analysis is very much useful for the telecom operators for optimizing the location of the BTS in virtual manner. This virtual drive test saves huge installation cost and also increases manpower cost.

The network simulations with the MIMO antenna element were carried out in the 4G and 5G bands. The data rate and throughput for a single stream, and two-stream scenarios over

the selected geographic region with the DPM model are tabulated in Tables 4 and 5. The full wave analysis using QPSK, 16 QAM, 64 QAM, and 256 QAM modulation schemes for both the DL and UL of the base station and the mobile station were carried out. According to the simulation results, the highest data rate and throughput are achieved with 256 QAM for base stations deployed at various BTS Sites 1, 2 and 3 locations.

The proposed base station antenna providing >40 dB isolation is used for the simulation and analysis of the deployed Band 41 (2.496–2.690 GHz) 4G cell sites with TDD wireless standards in the selected geographic area using the DPM and a comparison

Table 4. 4G (Band-41) radio network deployment parameters with a dominant path model

S. no.	Parameters	As per 3GPP expected values	4G	
			TDD	
			No MIMO stream	MIMO 2 stream
1	Received power (dBm)	—	-50	-50
2	DL: data rate (Mbps)	—	0.625	1.213
3	DL: throughput (Mbps)	—	62.53	119
4	UL: data rate (Kbps)	—	86.88	163.3
5	UL: throughput (Mbps)	—	7.688	15.63
6	Max. SNIR (dB)	≥ 20	40	55
7	RSRP (dBm)	≥ -80	-70	-75
8	RSRQ (dB)	≥ -15	-11	-11
9	RSSI (dBm)	≥ -65	-40	-40
10	Path loss (dB)	≤ -80	-90	-90

Table 5. 5G (Band-42) radio network deployment parameters with a dominant path model

S. no	Parameters	As per 3GPP expected values	5G			
			FDD		TDD	
			No MIMO stream	MIMO 2 streams	No MIMO stream	MIMO 2 stream
1	Received power (dBm)	—	-50	-50	-50	-50
2	DL: data rate (Mbps)	—	2.010	3.826	1.005	1.913
3	DL: throughput (Mbps)	—	548.6	1044	274.3	522.2
4	UL: data rate (Mbps)	—	1.548	2.8	0.774	1.473
5	UL: throughput (Mbps)	—	422.6	800	211.3	402.3
6	Maximum SNIR (dB)	≥ 20	45	50	45	45
7	RSRP (dBm)	≥ -80	-75	-75	-75	-75
8	RSRQ (dB)	≥ -15	-11	-4	-11	-4
9	RSSI (dBm)	≥ -65	-50	-40	-50	-40
10	Path loss (dB)	≤ -80	-90	-90	-90	-90

of the No MIMO stream and two-stream MIMO are made available. The data rates and throughput for both the UL and the DL are reported in Table 4. For the deployed cell sites, maximum DL data rate and throughput were 1.213 and 119 Mbps, respectively. The maximum UL data rate and throughput were 0.163 and 15.63 Mbps recorded with 20 MHz bandwidth with two-stream MIMO. The maximum received power and SNIR are -50 dBm and 55 dB and the maximum RSRP is -75 dBm, RSRQ is -11 dB, and RSSI is -40 dBm. DPM simulation results for the deployed Band 42 (3.4–3.6 GHz) 5G cell sites with FDD and TDD wireless standards with 100 MHz bandwidth in the selected geographic area are tabulated in Table 5. For the deployed cell sites, the maximum DL data rate and throughput were 3.826 and 1044 Mbps and the maximum UL data rate and throughput were 2.8 and 800 Mbps. The maximum received power and SNIR are -50 dBm and 50 dB, respectively, and the maximum RSRP is -75 dBm, RSRQ is -4 dB, and RSSI is -40 dBm.

Conclusion

A compact dual slant $\pm 45^\circ$ polarized MIMO antenna with high isolation for dual-generation BTS and vehicular base station

applications is presented. High isolation and low ECC are discovered by introducing a square metallic ring with a 3 mm air gap placed below the crisscrossed flared dipole radiators, which is connected to the dipole arm with the help of four shorting vias operating in Band 40/41/42/43. The proposed dual-polarized antenna height is $0.25\lambda_{3.5\text{GHz}}$. The prototype of a MIMO antenna element is fabricated and tested. Measured results show that the proposed dual-polarized antenna achieves 13.38% and 29.3% bandwidth in the Band 40/41 and sub-6 GHz bands, respectively. Simulated and measured results demonstrated that the proposed antenna offers stable radiation patterns with port-to-port isolation of >40 dB, with a maximum gain of 11.3 dBi and low XPD of -40 dB over the operating band. The WinProp platform is used to deploy the radiation patterns of the designed dual-polarized MIMO antenna element in the selected geographical area for detailed radio network planning. The maximum DL data rate and throughput were 3.826 and 1044 Mbps, respectively. The maximum UL data rate and throughput were 2.8 and 800 Mbps, respectively, with a two-stream MIMO antenna element for the deployed cell sites. The developed antenna is fit for the 4G and 5G sub-6 GHz MIMO BTS and vehicular base station antenna deployments.

Funding. Vadlamudi Roja and Sriram Kumar D. acknowledge the Ministry of Human Resource Development (MHRD), Government of India, to support a Research Grant through the Prime Minister's Research Fellowship (PMRF) Scheme, December 2020 Cycle.

Competing interest. The authors report no conflict of interest.

References

1. Andrews JG, Buzzi S, Choi W, Hanly SV, Lozano A, Soong AC and Zhang JC (2014) What will 5G be? *IEEE JSAC* 32(6), 1065–1082.
2. Wu PL and Chen X (2018) A broadband $\pm 45^\circ$ dual-polarized multiple-input multiple-output antenna for 5G base stations with extra decoupling elements. *Journal of Communications and Information Networks* 3(1), 31–37.
3. Vadlamudi R and Sriram Kumar D (2021) Nature enthused high isolation high gain miniaturized multiple-input multiple-output antenna for A-LTE/5G macro-cell base transceiver station applications. *International Journal of RF and Microwave Computer-Aided Engineering (RF-MCAD)* 31(12), e22885.
4. Zhang Q and Gao Y (2018) A compact broadband dual-polarized antenna array for base stations. *IEEE Antennas and Wireless Propagation Letters* 17(6), 1073–1076.
5. Wu W, Peng H and Mao J (2017) A new compact dual-polarized co-axial full-band antenna for 2G/3G/LTE base station applications. In *2017 IEEE Electrical Design of Advanced Packaging and Systems Symposium (EDAPS)*, 1–3.
6. Liu Y, Wang S, Li N, Wang J-B and Zhao J (2018) A compact dual-band dual-polarized antenna with filtering structures for sub-6 GHz base station applications. *IEEE Antennas and Wireless Propagation Letters* 17(10), 1764–1768.
7. Vadlamudi Roja, Ravi Kumar KRS *et al* (2019) A novel 3D miniaturized, wideband dual polarized antenna with high isolation, low cross polarization for A-LTE/5G base station applications. In *2019 TEQIP III Sponsored International Conference on Microwave Integrated Circuits, Photonics and Wireless Networks (IMICPW)*, IEEE, 392–395.
8. Wang W, Yang S, Fang Z, Sun Q, Chen Y and Zheng Y (2021) Compact dual-polarized wideband antenna with dual/single-band shifting for micro base station applications. *IEEE Transactions on Antennas and Propagation* 69(11), 7323–7332.
9. Huang H, Li X and Liu Y (2018) A novel vector synthetic dipole antenna and its common aperture array. *IEEE Transactions on Antennas and Propagation* 66(6), 3183–3188.
10. Hua Q, Huang Y, Alieldin A, Song C, Jia T and Xu Zhu A (2020) Dual-band dual-polarized base station antenna using a novel feeding structure for 5G communications. *IEEE Access* 8, 63710–63717.
11. Zhao L, Qian K-W and Wu K-L (2014) A cascaded coupled-resonator decoupling network for mitigating interference between two radios in adjacent frequency bands. *IEEE Transactions on Microwave Theory and Techniques* 62(11), 2680–2688.
12. Cui Y, Gao X, Fu H, Chu Q-X and Li R (2017) Broadband dual-polarized dual-dipole planar antennas: Analysis, design, and application for base stations. *IEEE Antennas and Propagation Magazine* 59(6), 77–87.
13. Yang S, Liang L, Wang W, Fang Z and Zheng Y (2021) Wideband gain enhancement of an AMC cavity-backed dual-polarized antenna. *IEEE Transactions on Vehicular Technology* 70(12), 12703–12712.
14. Luo Y, Chu Q-X and Wen D-L (2016) A plus/minus 45-degree dual-polarized base-station antenna with enhanced cross-polarization discrimination via the addition of four parasitic elements placed in a square contour. *IEEE Transactions on Antennas and Propagation* 64(4), 1514–1519.
15. Zheng D, Luo Y and Chu Q-X (2020) A miniaturized wideband dual-polarized antenna based on mode-control principle for base-station applications. *IEEE Access* 8, 62218–62227.
16. Zhang J, Yang K, Eide E, Yan S, and Vandenbosch GAE (2020) Simple triple-mode dual-polarized dipole antenna with small frequency separation ratio. *IEEE Antennas and Wireless Propagation Letters* 19(2), 262–266.
17. Donglin H, Chen Y and Yang S (2022) A low-profile triple-band shared-aperture antenna array for 5G base station applications. *IEEE Transactions on Antennas and Propagation* 70(4), 2732–2739.
18. <https://www.ansys.com/products/electronics/ansys-hfss> (accessed 25 June 2022).
19. Divya G, Jagadeesh Babu K and Madhu R (2021) A novel inverted elliptical frustum shaped multi-band MIMO DRA with bandwidth and isolation enhancement. *AEU: International Journal of Electronics and Communications* 135, 153725.
20. Divya G, Jagadeesh Babu K and Madhu R (2022) Isolation improvement in dual-band asteroid shaped MIMO DRA for LTE and ISM applications. *International Journal of RF and Microwave Computer-Aided Engineering* 32(1), e22929.
21. WinProp Wave propagation and radio network planning software (Part of Altair Hyper Works). <https://www.altair.com/> (accessed 4 May 2017).
22. <https://altairhyperworks.com/product/feko/winprop-propagation-modelling> (accessed 27 January 2022).
23. Wahl R and Wölfle G (2006) Combined Urban and indoor network planning using the dominant path propagation model. In *2006 First European Conference on Antennas and Propagation*, Nice, France, IEEE (accessed 6–10 November).
24. <https://sites.google.com/site/teencyclopedia/lte-radio-link-budgeting-and-rf-planning> (accessed 15 5 2021).
25. Khan MU, Abu Al-Saud WA and Sharawi MS (2014) Isolation enhancement effect on the measured channel capacity of a printed MIMO antenna system. In *The 8th European Conference on Antennas and Propagation (EuCAP 2014)*, Netherland, IEEE, 2834–2837



Roja Vadlamudi received B.Tech degree in Electronics and Communication Engineering in 2014 and M.Tech degree in 2016 from Acharya Nagarjuna University, Guntur, India. She was SPF (Senior Project Fellow) and JRF with the Indian Institute of Space Science and Technology, Indian Space Research Organization, Trivandrum, India, for 1.6 years. She was with the Radiant Tech. Pro. Pvt. Ltd, Bangalore, India, as an RF

and Antenna Engineer for 1.9 years. She is currently working toward her PhD thesis at National Institute of Technology, Tiruchirappalli. She received prestigious Prime Minister's Research Fellowship (PMRF) Award from MHRD Government of India in the Department of ECE, NIT Trichy. She has several publications in reputed International Journals and Conferences. She has a patent granted on "Dual-Generation MIMO Antenna with DB-BPF Characteristics for 4G and 5G BTS Applications and Method Thereof". She received 3 Best Paper Awards in IEEE 3rd WORLD 5G FORUM SUMMIT 2020 at Bangalore, IEEE IMICPW 2019, NIT Trichy, and Young Scientist's Conference as a part of India International Science Festival 2020, Delhi. She is a Student Member of IEEE and Antenna and Propagation-Society (AP-S) Madras Chapter, IEEE Young Professional, IEEE Council on RFID, IEEE Nanotechnology Council, IEEE Sensors Council, and IEEE Council on Electronic Design Automation. Her research interests are wideband antennas, metamaterials, reconfigurable antennas, RF and Microwave Circuits and Electromagnetic Band Gap Structures (EBG's), MIMO Antennas, massive MIMO Antennas, mm-wave Antennas, 5G/6G, and Beyond Technologies, THz Antennas, Conformal antennas for Space and Defense applications.



Sriram Kumar Dhamodharan is currently a professor in the Department of Electronics and Communication Engineering in National Institute of Technology, Tiruchirappalli, India. He received BE degree (1991) in Electronics and Communication Engineering, Thiagarajar College of Engineering, Madurai, India; ME degree (1993) with Distinction in Microwave and Optical Engineering, Alagappa Chettiar

College of Engineering and Technology, Karaikudi, India; and PhD degree (2009) in Microwave Integrated Circuits Coplanar Waveguide-Discontinuities, Periodic Structures Analysis, Antenna Applications, Bharathidasan University, Tiruchirappalli, India. He published numerous research papers in the International and National journals in the areas of microwave integrated circuits, optical networks, smart antennas, carbon nanotube antennas, free space optics, optical and reconfigurable antennas, flexible electronics, and photonics. He is a Senior Member IEEE.